

IL-17 is a neuromodulator of *Caenorhabditis elegans* sensory responses

Changchun Chen¹, Eisuke Itakura^{1†}, Geoffrey M. Nelson¹, Ming Sheng¹, Patrick Laurent^{1†}, Lorenz A. Fenk¹, Rebecca A. Butcher², Ramanujan S. Hegde¹ & Mario de Bono¹

Interleukin-17 (IL-17) is a major pro-inflammatory cytokine: it mediates responses to pathogens or tissue damage, and drives autoimmune diseases. Little is known about its role in the nervous system. Here we show that IL-17 has neuromodulator-like properties in *Caenorhabditis elegans*. IL-17 can act directly on neurons to alter their response properties and contribution to behaviour. Using unbiased genetic screens, we delineate an IL-17 signalling pathway and show that it acts in the RMG hub interneurons. Disrupting IL-17 signalling reduces RMG responsiveness to input from oxygen sensors, and renders sustained escape from 21% oxygen transient and contingent on additional stimuli. Over-activating IL-17 receptors abnormally heightens responses to 21% oxygen in RMG neurons and whole animals. IL-17 deficiency can be bypassed by optogenetic stimulation of RMG. Inducing IL-17 expression in adults can rescue mutant defects within 6 h. These findings reveal a non-immunological role of IL-17 modulating circuit function and behaviour.

The contributions of a neuron to circuit activity and behaviour depend on its responsiveness to upstream inputs, and its ability to drive downstream outputs. By modifying the input–output relationships between neurons, neuromodulators play crucial roles in information processing by the brain: they are thought to underlie changes in arousal, mood, and global animal states^{1–4}, and to contribute to learning and forgetting^{5,6}. Identifying neuromodulatory signalling pathways and understanding their *in vivo* effects on circuit function are important goals in understanding the neural basis for behaviour⁷.

The comparatively simple nervous system of *C. elegans* allows behaviours to be linked to small numbers of identified neurons connected by few, anatomically defined, chemical and electrical connections^{8,9} (<http://wormwiring.org>). Aggregation is an intricate behaviour of *C. elegans* governed by multiple sensory neurons, including receptors for O₂ (URX, AQR, PQR), noxious stimuli (ASH, ADL), food cues (ADF, ASK), and pheromones (ASJ, ADL, ASK)^{10–13}. Anatomically defined gap junctions connect the URX, ASH, ADL, and ASK neurons with RMG interneurons⁹, which process sensory information to control aggregation¹³. Here we use forward genetics to probe the molecular mechanisms regulating the properties of these neurons and connections.

IL-17 promotes aggregation of *C. elegans*

We mutagenized aggregating *npr-1* (null) (neuropeptide receptor 1) animals and identified more than 800 mutants that aggregated poorly but were otherwise overtly wild type. We sequenced the genomes of 583 mutants, and identified the lesions causing their aggregation defects. Six harboured mutations in Y64G10A.6, an interleukin-17 cytokine receptor orthologue we named *ilcr-1* (Extended Data Fig. 1a and Extended Data Table 1). An *ilcr-1* deletion, *tm5866*, disrupted aggregation and was rescued by expressing *ilcr-1* complementary DNA (cDNA) from the *ilcr-1* promoter (Fig. 1a). The *C. elegans* genome encodes a second IL-17-like receptor, F56D1.2, that we named *ilcr-2*. We did not identify *ilcr-2* alleles in our collection but CRISPR-generated *ilcr-2* nulls failed to aggregate (Fig. 1a and Extended Data Fig. 1a–d). Expressing *ilcr-2* cDNA from the *ilcr-2* promoter restored aggregation to *ilcr-2* but

not *ilcr-1* mutants, and vice versa (Fig. 1a and data not shown). Like their mammalian homologues¹⁴, ILCR-1 and ILCR-2 have an extracellular domain for ligand binding, a single transmembrane domain, and an intracellular SEF/IL-17R (SEFIR) signalling domain (Extended Data Fig. 1f).

Three *C. elegans* genes, *T22H6.1*, *F25D1.3*, and *C44B12.6*, share homology with mammalian IL-17 (Extended Data Fig. 1g and data not shown). We did not find alleles for *F25D1.3* or *C44B12.6* in our collection, and disrupting either gene did not perturb aggregation (Extended Data Fig. 1d, e). We found four alleles of *T22H6.1*, including splice-site mutations (Extended Data Table 1). Deletions of *T22H6.1*, *tm5124*, and *tm5218* disrupted aggregation, and were rescued by expressing *T22H6.1* cDNA from its promoter (Fig. 1a). *T22H6.1*, which we named *ilc-17.1* (interleukin-17 cytokine related gene 1), could therefore encode a ligand for ILCR-1/ILCR-2 receptors. Double and triple mutants of *ilc-17.1*, *ilcr-1*, and *ilcr-2* behaved like single mutants (Extended Data Fig. 1c and see below), suggesting these genes function in a single pathway.

Green fluorescent protein (GFP)-tagged ILCR-1 co-localized with haemagglutinin (HA)-tagged ILCR-2 at the plasma membrane of HEK293T cells (Fig. 1b), and ILCR-1–GFP specifically co-precipitated with ILCR-2–HA (Fig. 1c). Like mammalian IL-17s, ILC-17.1 formed disulfide-linked dimers¹⁵ (Extended Data Fig. 1h). ILC-17.1 specifically interacted with the surface of cells expressing ILCR-2, or ILCR-2 and ILCR-1, but not control cells, or cells expressing only ILCR-1 (Fig. 1d, e). In mammals, IL-17 binding to one receptor type is thought to increase affinity for the second receptor type, promoting heteromeric complex formation¹⁶. Together, our data suggest ILC-17.1 signals via ILCR-1/ILCR-2 co-receptors.

Aggregation of *C. elegans* is stimulated by 21% O₂, and many aggregation-defective mutants exhibit O₂ response defects^{12,17–19}. On bacterial food, *npr-1* animals respond to a 7–21% rise in O₂ by increasing their average speed from approximately 40 μm s⁻¹ to approximately 180 μm s⁻¹. This arousal is sustained for hours if animals are kept at 21% O₂, with only modest attenuation (Fig. 1f)²⁰. The *ilc-17.1*, *ilcr-1*, and *ilcr-2* mutants responded to 21% O₂ immediately after being transferred to the

¹MRC Laboratory of Molecular Biology, Francis Crick Avenue, Cambridge CB2 0QH, UK. ²Department of Chemistry, University of Florida, Gainesville, Florida 32611, USA. †Present addresses: Department of Nanobiology, Graduate School of Advanced Integration Science, Chiba University, Chiba, 263-8522, Japan (E.I.); Université Libre de Bruxelles, Laboratory of Neurophysiology, Campus Erasme, 808 Route de Lennik, 1070 Bruxelles, Belgium (P.L.).

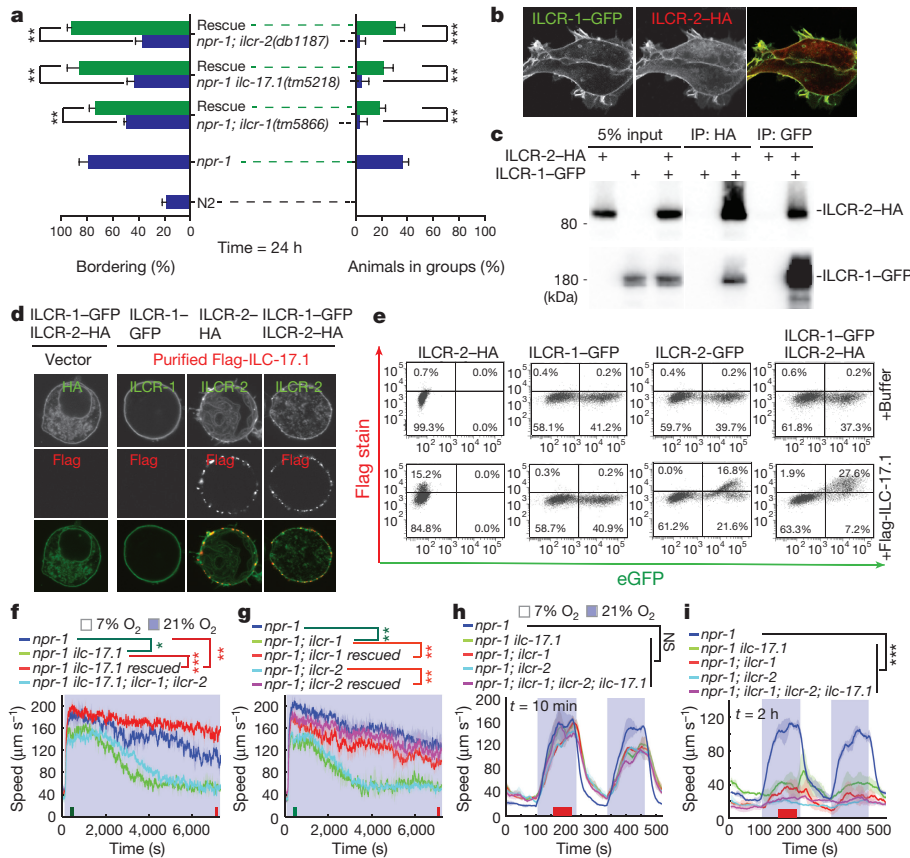


Figure 1 | IL-17 promotes aggregation and escape from 21% O₂. **a**, Bordering and aggregation phenotypes; $n = 4$ assays. $***P < 0.001$; $**P < 0.01$ (analysis of variance (ANOVA) with Tukey's correction). Data here and in all figures show mean \pm s.e.m. **b**, Cell surface expression of ILCR-1-GFP and ILCR-2-HA in HEK293T cells. **c**, Co-immunoprecipitation of ILCR-1 and ILCR-2. **d**, Flag-ILC-17.1 binding to receptor-transfected cells. **e**, Fluorescence-activated cell sorting of cells transfected with the indicated vector/s and exposed to

assay plates; however, unusually, their arousal declined to baseline within 1 h, and they became unresponsive to 21% O₂ thereafter (Fig. 1f–i). These defects could be rescued by expressing the corresponding wild-type gene either from extrachromosomal multicopy arrays (Fig. 1f, g) or by a single copy insertion²¹ (Extended Data Fig. 1i). Knocking out *ilcr-1* or *ilcr-2* in animals carrying the natural *npr-1* 215F allele recapitulated the defects we observed in *npr-1*(null) mutants (Extended Data Fig. 1j).

IL-17 increases RMG interneuron gain

Functional ILCR-1 and ILCR-2 receptors that were carboxy (C)-terminally tagged with GFP were expressed in most neurons, including RMG interneurons (Fig. 2a–d). We found *ilcr-2* was also expressed in pharyngeal muscle. Selectively expressing *ilcr-1* or *ilcr-2* cDNA in the O₂ sensors, using the *gcy-32* promoter, only weakly rescued *ilcr* mutant phenotypes (Extended Data Fig. 2a–d). By contrast, expressing receptors in RMG, using the *npr-1* or *flp-5* promoters, robustly restored persistent escape from 21% O₂ and aggregation to *ilcr* mutants (Extended Data Fig. 2a–d). The *flp-5* promoter drives expression in ASG (previously reported as ASE)²² and RMG, but expressing *ilcr-1* cDNA in ASG using the *ops-1* promoter did not rescue *ilcr-1* phenotypes (Extended Data Fig. 2e); neither did expression in cholinergic neurons (*unc-17* or *acr-2* promoters), GABAergic neurons (*unc-25* promoter), or interneurons controlling forward and reverse movement (*glr-1* or *nmr-1* promoters) (Extended Data Fig. 2f). To confirm RMG as the focus of action, we inserted a single copy of *ilcr-1* in which a strong terminator of transcription, flanked by LoxP sites, separated the promoter and open reading frame. As expected,

Flag-ILC-17.1 or buffer. **f**, **g**, Average speed of animals kept 2 min at 7% O₂ then 2 h at 21% O₂. Rescue lines are as in **a**. Here and hereafter, time intervals at 7% O₂ are open, shading indicates 21% O₂, and green and red bars on the x axis indicate intervals used for statistics; $n = 4$ assays, 120 animals. $*P < 0.05$, $**P < 0.01$, and $***P < 0.001$, Mann-Whitney *U*-test. **h**, **i**, Speed at 7% and 21% O₂ assayed 10 min (**h**) or 2 h (**i**) after animals were transferred to assay plates; $n = 3$ assays, 90 animals. NS, not significant, $***P < 0.001$, Mann-Whitney *U*-test.

this transgene did not rescue the *ilcr-1* mutant phenotype unless we also selectively expressed Cre recombinase in RMG, using the *flp-5* or *npr-1* promoters (Fig. 2e). These data suggest the ILCR co-receptors act predominantly in the RMG interneurons to promote aggregation and escape from 21% O₂.

Functional mCherry-tagged ILC-17.1 accumulated in coelomocytes, scavenger cells that endocytose macromolecules from the body cavity of *C. elegans*²³, confirming that ILC-17.1 is secreted (Fig. 2f, top panels). A functional bicistronic construct co-expressing *ilcr-17.1* and free mCherry labelled the RMG, AUA, and ASE neurons (Fig. 2f, bottom panels). Targeted expression of *ilcr-17.1* in RMG restored the O₂ response, suggesting the ligand could act as an autocrine signal (Extended Data Fig. 2g). However, expressing *ilcr-17.1* in the AWA olfactory neurons or the ASE gustatory neurons also rescued the *ilcr-17.1* mutant phenotype (Extended Data Fig. 2h), suggesting the ligand source is unimportant. Expression and release of ILC-17.1 from RMG appears to be O₂-independent: mCherry-ILC-17.1 accumulation in coelomocytes was similar in animals cultivated at 7% and 21% O₂ (Fig. 2g), as were RMG levels of cytoplasmic mCherry expressed from the bicistronic *pilc-17.1::ilcr-17.1::sl2::mCherry* transgene (data not shown). Constitutive *ilcr-17.1* expression from the *ges-1* or *vha-6* gut-specific promoters rescued the *ilcr-17.1* defects (Fig. 2h). The O₂-regulated behaviour of these transgenic animals suggests *ilcr-17.1* does not itself drive arousal, and can promote O₂ circuit function without being regulated by O₂. However, this does not exclude the possibility that *ilcr-17.1* expression, or its effects on RMG, are regulated by interacting inputs, as happens in the mammalian immune system^{24,25}.

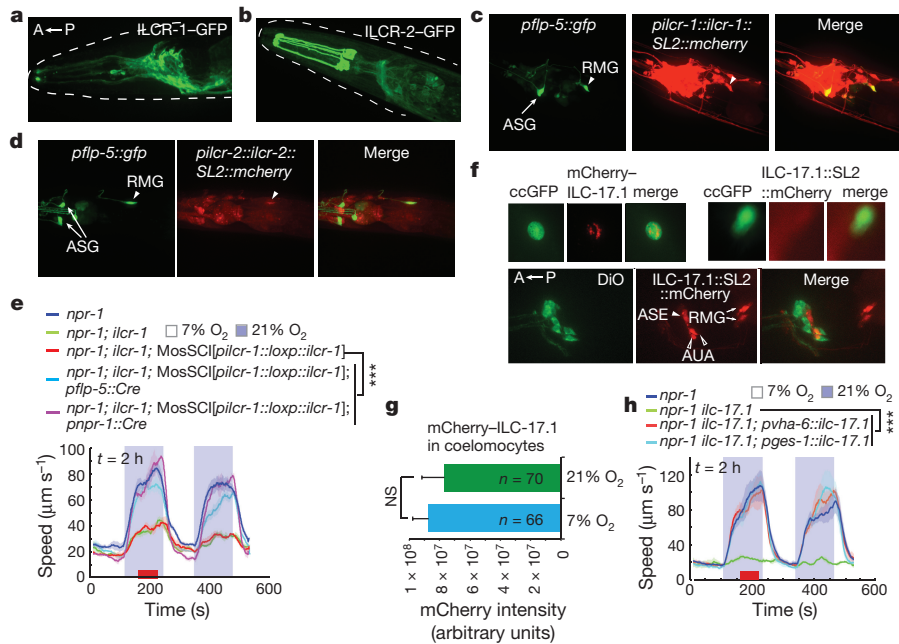


Figure 2 | Anatomical focus of ILC-17.1 signalling. **a–d**, *ilcr-1-gfp* and *ilcr-2-gfp* are expressed in many neurons (**a**, **b**), including RMG, identified using *pflp-5::gfp* (**c**, **d**). **e**, O₂ response defects in *ilcr-1* rescued by selective expression in RMG (*pilcr-1* and *pflp-5*); *n* = 4 assays, 120 animals. ****P* < 0.001, Mann–Whitney *U*-test. **f**, ILC-17.1 expression. Top left, functional mCherry–ILC-17.1 accumulates in coelomocytes (labelled with GFP, ccGFP). Top right, a functional *pilcr-17.1::ilc-17.1::SL2::mCherry*

polycistronic transgene does not highlight coelomocytes but (bottom) labels the RMG, AUA, and ASE neurons. DiO-labelled neurons provide reference points. A, anterior; P, posterior. **g**, mCherry–ILC-17.1 accumulation in coelomocytes is not O₂ dependent. NS, not significant by *t*-test. **h**, Gut-specific expression of *ilc-17.1* cDNA rescues *ilc-17.1* defects; *n* = 4 assays, 120 animals. ****P* < 0.001, Mann–Whitney *U*-test.

To test whether ILC-17.1 altered RMG responsiveness to input from O₂ sensors, we used YC2.60 Ca²⁺ sensors²⁶ to image RMG and URX (as a control) in freely moving animals under our behavioural assay conditions. URX Ca²⁺ responses to 21% O₂ were not altered in *ilc-17.1* or *ilcr-2* mutants compared with controls, either 10 min or 2 h after animals were picked onto the assay plate (Fig. 3a). By contrast, RMG Ca²⁺ responses to 21% O₂ were reduced at both time points in

mutants (Fig. 3b). Expressing *ilcr-2* in RMG rescued these defects in *ilc-17.1* mutants (Extended Data Fig. 2i). Imaging RMG in an *npr-1* 215F background revealed similar phenotypes to those in *npr-1* null mutants (Extended Data Fig. 2j). As an independent assay of RMG activity we measured *pflp-5::gfp* expression (FMRFamide-like neuropeptide) in RMG. Expression from this neuropeptide reporter increases with RMG activity²⁷. The *ilc-17.1*, *ilcr-1*, and *ilcr-2* mutants kept at 21% O₂

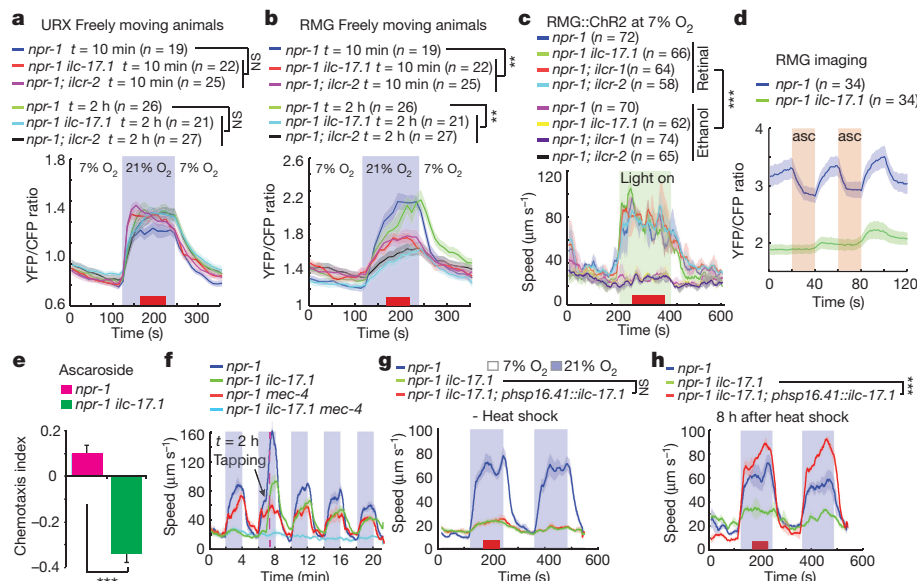


Figure 3 | ILC-17.1 signalling alters RMG physiology. **a**, **b**, O₂-evoked Ca²⁺ responses in URX (**a**) and RMG (**b**). ***P* < 0.01, Mann–Whitney *U*-test. **c**, Effect of stimulating RMG using channelrhodopsin in animals kept at 7% O₂. ****P* < 0.001, NS, not significant, Mann–Whitney *U*-test. **d**, **e**, Disrupting *ilc-17.1* reduces ascarioside-evoked (asc) responses in RMG (**d**) and switches valence of ascarioside pheromones (**e**). For **e**, *n* = 9 assays; ****P* < 0.001, *t*-test. **f**, Tapping restores responsiveness

to 21% O₂ in *ilc-17.1* mutants. The arrow and purple line indicate taps to the microscope stage at 7 min. The *mec-4* mutants are touch insensitive. For **f**, *n* = 4 assays, 120 animals. **g**, **h**, Heat-shock-induced expression in adults rescues *ilc-17.1* O₂ responses. Assays were performed 2 h after heat-shock; *n* = 4 assays, 120 animals. ****P* < 0.001, Mann–Whitney *U*-test.

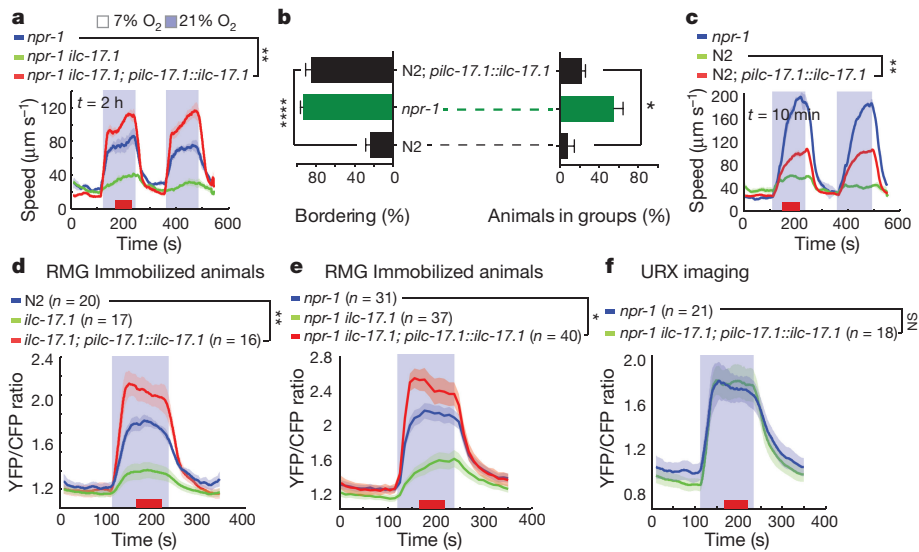


Figure 4 | Overexpressing ILC-17.1 heightens responsiveness to 21% O₂. **a**, Animals overexpressing ILC-17.1 respond more strongly to 21% O₂ than *npr-1* control animals; $n = 4$ assays, 120 animals. $**P < 0.01$, Mann–Whitney *U*-test. **b**, Overexpressing ILC-17.1 in N2 animals promotes bordering and aggregation; $n = 4$ assays. $*P < 0.05$, $****P < 0.0001$, *t*-test. **c**, N2 animals overexpressing ILC-17.1 show increased responsiveness to

21% O₂; $n = 4$ assays, 120 animals. $**P < 0.01$, Mann–Whitney *U*-test. **d–f**, ILC-17.1 overexpression increases O₂-evoked Ca²⁺ responses in RMG in N2 (**d**) and *npr-1* (**e**) animals, but does not alter O₂-evoked Ca²⁺ responses in URX (**f**). $*P < 0.05$; $**P < 0.01$, Mann–Whitney *U*-test. YFP, yellow fluorescent protein; CFP, cyan fluorescent protein.

showed reduced *pflp-5::gfp* fluorescence compared with *npr-1* controls, consistent with reduced RMG activity (Extended Data Fig. 2k). Disrupting *ilc-17.1* reduced RMG responsiveness to O₂ input without compromising its ability to signal to downstream neurons: stimulating RMG using channelrhodopsin evoked similar behavioural responses in *ilc-17.1* mutants and control animals (Fig. 3c).

RMG interneurons influence the pheromone responses of *C. elegans*, and are coupled by gap junctions to ASK and ADL pheromone-responsive neurons^{9,13,28}. Using Ca²⁺ imaging we found that a mixture of C3 + C6 + C9 ascarosides^{29,30} evoked a response in RMG reminiscent of that evoked by the same ascaroside mix in ASK neurons¹³. This response was strongly reduced in *ilc-17.1* mutants (Fig. 3d), perhaps because RMG neurons have lower Ca²⁺ at 21% O₂. Moreover, unlike *npr-1* animals, which are attracted to this ascaroside mix¹³, *ilc-17.1* mutants were repelled by it (Fig. 3e). Thus, ILC-17.1 signalling influences pheromone responses.

IL-17 signalling components are expressed broadly in the nervous system. Do they affect all behavioural responses? The *ilc-17.1* mutants showed normal chemotaxis to NaCl, mediated by the ASE neurons, and benzaldehyde, mediated by AWC, and did not alter benzaldehyde-evoked Ca²⁺ responses in AIB interneurons (Extended Data Fig. 2l–n). Thus, IL-17 defects do not cause general circuit dysfunction.

Why do mutants with chronic defects in the RMG responsiveness to 21% O₂ escape this cue 10 min, but not 2 h, after being picked for assay? We speculated that physically transferring animals, which stimulates mechanoreceptors, transiently makes reduced RMG output sufficient to drive escape from 21% O₂. Mechanosensory stimulation is known to transiently increase locomotor speed through activation of gentle touch neurons (Y. Tanizawa, B. Zhao and W. Schafer, personal communication). Consistent with our hypothesis, gently tapping the microscope stage 2 h after transferring animals for assay instantly restored responsiveness to 21% O₂ to *ilc* signalling mutants, as long as their gentle touch receptors were functional (Fig. 3f). Thus, without *ilc-17.1* signalling, *C. elegans* requires additional sensory stimulation to escape 21% O₂.

Heat-shock-induced expression of *ilc-17.1*, *ilcr-1*, or *ilcr-2* cDNA in adults rescued the respective mutant (Fig. 3g, h and Extended Data Fig. 3). Experiments in which we changed heat-shock duration while monitoring expression of a *pbsp-16.41::ilc-17.1::mCherry* bicistronic transgene and O₂ responses suggested that ILC-17.1 signalling requires

less than 6 h to exert its effects (Extended Data Fig. 4). Faster induction of ILC-17.1 expression using longer heat shock did not shorten the time required for rescue.

Elevating IL-17 heightens O₂ responses

Animals overexpressing *ilc-17.1* from its own promoter, the *hsp-16.41*, *flp-5*, *odr-10* (AWA), *flp-6* (ASE), or gut promoters all showed abnormally heightened responses to 21% O₂ (Figs. 1f and 4a and Extended Data Figs 2g, h and 4). Moreover, overexpressing *ilc-17.1* in the non-aggregating N2 laboratory strain conferred aggregation behaviour and responsiveness to 21% O₂ (Fig. 4b, c). Neural imaging showed that ILC-17.1 overexpression significantly increased RMG Ca²⁺ responses, both in N2 and in *npr-1* animals (Fig. 4d, e). It also increased *pflp-5::gfp* expression in RMG in N2 and *npr-1* animals kept at 21% O₂, consistent with increased RMG output (Extended Data Fig. 5). However, animals overexpressing *ilc-17.1* behaved appropriately at 7% O₂, and had unaltered RMG Ca²⁺ levels at 7% O₂, suggesting ILC-17.1 overexpression did not itself depolarize RMG. O₂-evoked responses in RMG depend on URX²⁷. Overexpressing *ilc-17.1* did not alter O₂-evoked Ca²⁺ response in URX (Fig. 4f).

An IL-17 signalling pathway in neurons

A candidate approach did not identify components acting downstream of the ILC-17.1 receptors (Extended Data Fig. 6). We therefore screened our collection for mutants exhibiting the unusual *ilc-17.1* O₂-response defect. Eight strains had such defects, highlighting three genes. One gene encoded an Act1 homologue we named *actl-1* (Act1-like) (Extended Data Fig. 7). Mammalian Act1 binds IL-17 receptors via SEFIR–SEFIR domain interactions and mediates their signalling output³¹. ACTL-1 has the Death domain/linker/SEFIR domain architecture found in non-vertebrate Act1 homologues, and lacks the helix–loop–helix and U-box found in mammalian Act1 (Extended Data Fig. 7e, f)³². Pull-downs from HEK293T cells co-expressing ACTL-1, ILCR-1, and ILCR-2 showed that ACTL-1 physically interacts with ILCR-1/ILCR-2, primarily via association with ILCR-2 (Fig. 5a, b)—consistent with ACTL-1 being an adaptor for *C. elegans* IL-17 receptors. The second gene encoded the sole *C. elegans* IRAK (interleukin-1 receptor-associated kinase) *pik-1* (Extended Data Fig. 8)³³. PIK-1–Flag and ACTL-1–HA co-expressed in HEK cells formed a complex (Fig. 5c, d), suggesting these two proteins interact physically. The

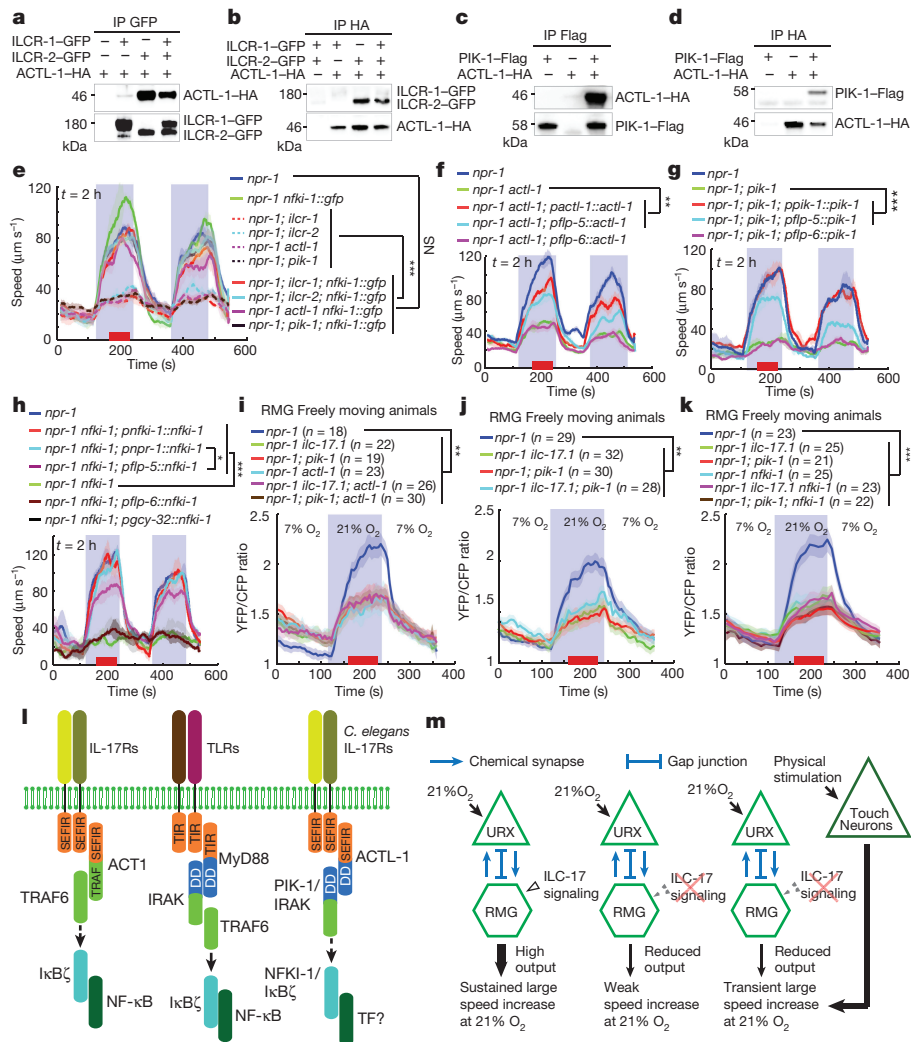


Figure 5 | ACTL-1, PIK-1/IRAK, and NFKI-1 mediate ILC-17.1 signalling in RMG. **a, b**, Immunoprecipitation of ILCR-1-GFP and ILCR-2-GFP co-immunoprecipitated ACTL-1-HA (**a**). Conversely, immunoprecipitation of ACTL-1-HA pulled down ILCR-2-GFP and, more weakly, ILCR-1-GFP (**b**). **c, d**, Immunoprecipitation of PIK-1-Flag pulled down ACTL-1-HA (**c**). Overexpression of ACTL-1-HA pulled down PIK-1-Flag (**d**). **e**, Overexpressing NFKI-1 rescues the O₂ response defects of *ilcr-1*, *ilcr-2*, *actl-1*, and *pik-1* mutants; *n* = 4 assays, 120 animals. ****P* < 0.001, Mann-Whitney *U*-test. **f-h**, The *actl-1* (**f**), *pik-1* (**g**), and *nfki-1* (**h**) O₂ response defects can be rescued by selectively expressing the corresponding cDNA in RMG interneurons (*pnp-1* and

pflp-5) but not URX, AQR, and PQR (*pgcy-32*) or ASE (*pflp-6*) sensory neurons (*n* = 4 assays, 120 animals). **P* < 0.05, ****P* < 0.001, Mann-Whitney *U*-test. **i-k**, O₂-evoked Ca²⁺ responses in RMG of single and double null mutants of *ilc-17.1*, *actl-1*, *pik-1*, and *nfki-1*. ***P* < 0.01, ****P* < 0.001, Mann-Whitney *U*-test. **l**, ILC-17.1 signalling in *C. elegans* compared with IL-17 and Toll-like receptor (TLR) pathways in mammals. TF, transcription factor. **m**, Model. ILC-17.1 increases RMG responsiveness to input from the URX O₂ sensors, enabling *C. elegans* arousal at 21% O₂. Without ILC-17.1, *C. elegans* responds poorly to 21% O₂ unless also mechanically stimulated.

remaining gene encodes the sole *C. elegans* homologue of the atypical IκB NF-κB inhibitors NFKBID and NFKBIZ/IκBζ³⁴⁻³⁶, which we called *nfki-1* (Extended Data Fig. 9). In mammals, IκBζ contributes to immune responses mediated by IL-1β, Toll-like receptors, and IL-17, but its *in vivo* functions are poorly understood^{37,38}. The *actl-1*, *pik-1*, or *nfki-1* mutant defects could be rescued by a single-copy insertion of the corresponding wild-type gene generated by MosSCI (Extended Data Fig. 7c). Various double mutants of *ilc-17.1*, *actl-1*, *pik-1*, and *nfki-1* did not show enhanced behavioural phenotypes (Extended Data Fig. 7-9), suggesting their gene products act in the same pathway. Overexpressing wild-type *nfki-1* restored aggregation and sustained escape from 21% O₂ to *ilcr-1*, *ilcr-2*, *actl-1*, and *pik-1* null mutants (Fig. 5e), suggesting that NFKI-1 acts downstream of these signalling components.

Many neurons including RMG showed expression of *actl-1*, *pik-1*, and *nfki-1* (Extended Data Figs 8d and 9c and data not shown). Expressing their cDNA in RMG using the *pnp-1* promoter rescued the mutant phenotype of each gene (Fig. 5f-h), although not completely. Expressing one or more of *actl-1*, *pik-1*, or *nfki-1* from the *ops-1* (ASG

neurons), *gcy-32* (AQR, PQR and URX), or *flp-6* (ASE) promoters failed to rescue the corresponding mutant phenotypes, whereas expressing *nfki-1* from the *npr-1* promoter, which drives expression in RMG and other neurons, rescued *nfki-1* phenotypes (Fig. 5f-h). Incomplete rescue of the *pflp-5*-driven transgenes suggests these genes may act in other neurons besides RMG to regulate O₂ responses, especially since the more broadly expressed *npr-1* promoter conferred significantly better rescue of the *nfki-1* phenotype (Fig. 5h). However, we cannot exclude other explanations, such as variability across transgenes.

Ca²⁺ imaging experiments showed that *actl-1*, *pik-1*, and *nfki-1* mutants recapitulate *ilc-17.1* phenotypes: reduced RMG responsiveness to 21% O₂ (Fig. 5i-k). The RMG Ca²⁺ response defects were non-additive in various double-mutant combinations of *ilc-17.1*, *actl-1*, *pik-1*, and *nfki-1* (Fig. 5i-k), as expected if the products of these genes function together in a signalling pathway. The ILCR-1/2-ACTL-1-PIK-1/IRAK relationship is reminiscent of Toll-like and IL-1β receptor signalling pathways, in which the adaptor MyD88 recruits IRAKs via homotypic Death domain interactions (Fig. 5l). TIR and SEFIR

domains are related domains³⁹. Consistent with this evolutionary relationship, in the mammalian immune system IL-17 and TLR receptor pathways activate similar downstream genes¹⁴. The aggregation and arousal of *C. elegans* at 21% O₂ are influenced by the presence of bacteria, and modulate pathogen responses⁴⁰. Plausibly, IL-17 signalling may have played a role in ancient nervous systems regulating behavioural responses to bacteria.

Conclusions

IL-17 is a potent pro-inflammatory cytokine. Its production in mammals is induced by infection, tissue damage, and stress, and is thought to drive tissue inflammation and autoimmune disease. By contrast, its roles in regulating neural circuit functions are elusive, although members of the IL-17 and IL-17 receptor family are expressed in brain¹⁴. Our data show that physiological levels of IL-17 can act directly on neurons to increase their responsiveness to presynaptic input. Elevating IL-17 levels can abnormally increase circuit sensitivity to O₂ input. By potentiating circuit function, IL-17 signalling transforms an escape response to a noxious cue from one that is transient and contingent on other sensory inputs, to one that is unconditional and sustained (Fig. 5m).

Online Content Methods, along with any additional Extended Data display items and Source Data, are available in the online version of the paper; references unique to these sections appear only in the online paper.

Received 13 May; accepted 23 November 2016.

Published online 18 January 2017.

- Marder, E. Neuromodulation of neuronal circuits: back to the future. *Neuron* **76**, 1–11 (2012).
- Root, C. M., Ko, K. I., Jafari, A. & Wang, J. W. Presynaptic facilitation by neuropeptide signaling mediates odor-driven food search. *Cell* **145**, 133–144 (2011).
- Lee, S. H. & Dan, Y. Neuromodulation of brain states. *Neuron* **76**, 209–222 (2012).
- Su, C. Y. & Wang, J. W. Modulation of neural circuits: how stimulus context shapes innate behavior in *Drosophila*. *Curr. Opin. Neurobiol.* **29**, 9–16 (2014).
- Owald, D. & Waddell, S. Olfactory learning skews mushroom body output pathways to steer behavioral choice in *Drosophila*. *Curr. Opin. Neurobiol.* **35**, 178–184 (2015).
- Cohn, R., Morantte, I. & Ruta, V. Coordinated and compartmentalized neuromodulation shapes sensory processing in *Drosophila*. *Cell* **163**, 1742–1755 (2015).
- McCormick, D. A. & Nusbaum, M. P. Editorial overview: neuromodulation: tuning the properties of neurons, networks and behavior. *Curr. Opin. Neurobiol.* **29**, iv–vii (2014).
- Chalfie, M. *et al.* The neural circuit for touch sensitivity in *Caenorhabditis elegans*. *J. Neurosci.* **5**, 956–964 (1985).
- White, J. G., Southgate, E., Thomson, J. N. & Brenner, S. The structure of the nervous system of the nematode *Caenorhabditis elegans*. *Phil. Trans. R. Soc. Lond. B* **314**, 1–340 (1986).
- de Bono, M., Tobin, D. M., Davis, M. W., Avery, L. & Bargmann, C. I. Social feeding in *Caenorhabditis elegans* is induced by neurons that detect aversive stimuli. *Nature* **419**, 899–903 (2002).
- Coates, J. C. & de Bono, M. Antagonistic pathways in neurons exposed to body fluid regulate social feeding in *Caenorhabditis elegans*. *Nature* **419**, 925–929 (2002).
- Gray, J. M. *et al.* Oxygen sensation and social feeding mediated by a *C. elegans* guanylate cyclase homologue. *Nature* **430**, 317–322 (2004).
- Macosko, E. Z. *et al.* A hub-and-spoke circuit drives pheromone attraction and social behaviour in *C. elegans*. *Nature* **458**, 1171–1175 (2009).
- Gaffen, S. L. Structure and signalling in the IL-17 receptor family. *Nature Rev. Immunol.* **9**, 556–567 (2009).
- Hymowitz, S. G. *et al.* IL-17s adopt a cystine knot fold: structure and activity of a novel cytokine, IL-17F, and implications for receptor binding. *EMBO J.* **20**, 5332–5341 (2001).
- Ely, L. K., Fischer, S. & Garcia, K. C. Structural basis of receptor sharing by interleukin 17 cytokines. *Nature Immunol.* **10**, 1245–1251 (2009).
- Cheung, B. H., Cohen, M., Rogers, C., Albayram, O. & de Bono, M. Experience-dependent modulation of *C. elegans* behavior by ambient oxygen. *Curr. Biol.* **15**, 905–917 (2005).
- Rogers, C., Persson, A., Cheung, B. & de Bono, M. Behavioral motifs and neural pathways coordinating O₂ responses and aggregation in *C. elegans*. *Curr. Biol.* **16**, 649–659 (2006).
- Persson, A. *et al.* Natural variation in a neural globin tunes oxygen sensing in wild *Caenorhabditis elegans*. *Nature* **458**, 1030–1033 (2009).
- Busch, K. E. *et al.* Tonic signaling from O₂ sensors sets neural circuit activity and behavioral state. *Nature Neurosci.* **15**, 581–591 (2012).
- Frøkjær-Jensen, C. *et al.* Random and targeted transgene insertion in *Caenorhabditis elegans* using a modified Mos1 transposon. *Nature Methods* **11**, 529–534 (2014).
- Kim, K. & Li, C. Expression and regulation of an FMRFamide-related neuropeptide gene family in *Caenorhabditis elegans*. *J. Comp. Neurol.* **475**, 540–550 (2004).
- Fares, H. & Greenwald, I. Genetic analysis of endocytosis in *Caenorhabditis elegans*: coelomocyte uptake defective mutants. *Genetics* **159**, 133–145 (2001).
- Gaffen, S. L. Recent advances in the IL-17 cytokine family. *Curr. Opin. Immunol.* **23**, 613–619 (2011).
- Iwakura, Y., Ishigame, H., Saijo, S. & Nakae, S. Functional specialization of interleukin-17 family members. *Immunity* **34**, 149–162 (2011).
- Nagai, T., Yamada, S., Tominaga, T., Ichikawa, M. & Miyawaki, A. Expanded dynamic range of fluorescent indicators for Ca²⁺ by circularly permuted yellow fluorescent proteins. *Proc. Natl Acad. Sci. USA* **101**, 10554–10559 (2004).
- Laurent, P. *et al.* Decoding a neural circuit controlling global animal state in *C. elegans*. *eLife* **4**, 04241 (2015).
- Jang, H. *et al.* Neuromodulatory state and sex specify alternative behaviors through antagonistic synaptic pathways in *C. elegans*. *Neuron* **75**, 585–592 (2012).
- Butcher, R. A., Fujita, M., Schroeder, F. C. & Clardy, J. Small-molecule pheromones that control dauer development in *Caenorhabditis elegans*. *Nature Chem. Biol.* **3**, 420–422 (2007).
- Butcher, R. A., Ragains, J. R., Kim, E. & Clardy, J. A potent dauer pheromone component in *Caenorhabditis elegans* that acts synergistically with other components. *Proc. Natl Acad. Sci. USA* **105**, 14288–14292 (2008).
- Qian, Y. *et al.* The adaptor Act1 is required for interleukin 17-dependent signaling associated with autoimmune and inflammatory disease. *Nature Immunol.* **8**, 247–256 (2007).
- Ryzhakov, G., Blazek, K. & Udalova, I. A. Evolution of vertebrate immunity: sequence and functional analysis of the SEFIR domain family member Act1. *J. Mol. Evol.* **72**, 521–530 (2011).
- Pujol, N. *et al.* A reverse genetic analysis of components of the Toll signaling pathway in *Caenorhabditis elegans*. *Curr. Biol.* **11**, 809–821 (2001).
- Kitamura, H., Kanehira, K., Okita, K., Morimatsu, M. & Saito, M. MAIL, a novel nuclear I κ B protein that potentiates LPS-induced IL-6 production. *FEBS Lett.* **485**, 53–56 (2000).
- Haruta, H., Kato, A. & Todokoro, K. Isolation of a novel interleukin-1-inducible nuclear protein bearing ankyrin-repeat motifs. *J. Biol. Chem.* **276**, 12485–12488 (2001).
- Yamazaki, S., Muta, T. & Takeshige, K. A novel I κ B protein, I κ B- ζ , induced by proinflammatory stimuli, negatively regulates nuclear factor- κ B in the nuclei. *J. Biol. Chem.* **276**, 27657–27662 (2001).
- Kao, C. Y., Kim, C., Huang, F. & Wu, R. Requirements for two proximal NF- κ B binding sites and I κ B- ζ in IL-17A-induced human β -defensin 2 expression by conducting airway epithelium. *J. Biol. Chem.* **283**, 15309–15318 (2008).
- Karlsen, J. R., Borregaard, N. & Cowland, J. B. Induction of neutrophil gelatinase-associated lipocalin expression by co-stimulation with interleukin-17 and tumor necrosis factor- α is controlled by I κ B- ζ but neither by C/EBP- β nor C/EBP- δ . *J. Biol. Chem.* **285**, 14088–14100 (2010).
- Novatchkova, M., Leibbrandt, A., Werzowa, J., Neubüser, A. & Eisenhaber, F. The STIR-domain superfamily in signal transduction, development and immunity. *Trends Biochem. Sci.* **28**, 226–229 (2003).
- Meisel, J. D. & Kim, D. H. Behavioral avoidance of pathogenic bacteria by *Caenorhabditis elegans*. *Trends Immunol.* **35**, 465–470 (2014).

Supplementary Information is available in the online version of the paper.

Acknowledgements We thank the *Caenorhabditis* Genetics Center (funded by National Institutes of Health Infrastructure Program P40 OD010440) and the Japanese knockout consortium for strains, J. Hadfield and the Cambridge Research Institute Genomics Core for whole genome sequencing, Z. Soltesz for software, B. Gyenes for help screening for mutants, S. Flynn for help with mapping, and de Bono laboratory members for comments on the manuscript. This work was supported by a European Molecular Biology Organization Fellowship (to C.C.), a Japan Society for the Promotion of Science Post-doctoral Fellowship (to E.I.), the Medical Research Council, UK, and the European Research Council (Advanced Grant 269058) to M.d.B.

Author Contributions C.C., E.I., R.S.H., and M.d.B. designed experiments. C.C., E.I., M.S., P.L., and L.A.F. performed experiments. G.N. did the genome sequence data analysis. R.A.B. provided reagents. C.C., E.I., R.S.H., and M.d.B. analysed the data. C.C. and M.d.B. wrote the paper.

Author Information Reprints and permissions information is available at www.nature.com/reprints. The authors declare no competing financial interests. Readers are welcome to comment on the online version of the paper. Correspondence and requests for materials should be addressed to M.d.B. (debono@mrc-lmb.cam.ac.uk).

Reviewer Information *Nature* thanks R. Garcia, O. Hobert and the other anonymous reviewer(s) for their contribution to the peer review of this work.

METHODS

No statistical methods were used to predetermine sample size. The experiments were not randomized.

Strains. *C. elegans* were maintained under standard conditions⁴¹. All assays used young (<1 day old) adult hermaphrodites. A detailed description of the forward genetic screens will be published elsewhere. The molecular lesions in alleles identified by forward genetics are listed in Extended Data Table 1. Frameshift mutations were generated using CRISPR-Cas9, as described⁴². Strains used are listed in Supplementary Table 1.

Behavioural assays. Aggregation and locomotion were assayed as described previously^{27,43}, with slight alterations. L4 animals were picked to a fresh plate 24 h before assay. Sixty animals were re-picked to the assay plate (an NGM plate seeded 2 days earlier with a 1-cm diameter OP50 lawn), and bordering and aggregation scored 2 and 24 h later. The scorer was blind to genotype. To assay locomotion we tracked 30 animals 10 min and 2 h after picking. We took care not to accidentally tap plates at the 2-h time point. For behavioural assays lasting 9 min, statistical comparisons used a 1-min window that started 40 s after the switch from 7% to 21% O₂ and stopped 20 s before the switch from 21% to 7% O₂. For the 2-h-long experiments, statistical comparisons used two 5-min windows, which started 5 min after the switch from 7% to 21% O₂, and 10 min before the assay ended. These intervals were sufficiently long to smooth out short-term fluctuations and highlight longer-term trends, while avoiding time periods when animals were rapidly changing their behaviour in response to the O₂ stimulus. Movies were analysed using Zentracker, a custom-written Matlab software (code available at <https://github.com/wormtracker/zentracker>). All worms in the field of view were analysed except those in contact with other animals. Speed was calculated as instantaneous worm centroid displacement between successive frames, and plotted as mean ± s.e.m. Behavioural responses were robust: three or four biological replicates (each including 60 animals) for aggregation assays, and 30 animals for locomotion assays, provided sufficient statistical power to distinguish phenotypes. Statistical comparisons for speed assays used a two-tailed Mann–Whitney *U*-test.

For quadrant chemotaxis assays, chemotaxis to a mixture of C3, C6, and C9 ascarosides, each at 10 nM, was assayed as described previously¹³. Briefly, about 2 h before the assay, 200 adult animals were picked to a fresh plate seeded with OP50. For the assay, animals were washed three times in chemotaxis buffer (1 mM CaCl₂, 1 mM MgSO₄, and 5 mM KH₂PO₄/K₂HPO₄ pH 6.0) then placed in the centre of the quadrant assay plate. Assay plates were freshly made with ascarosides added to alternate quadrants. The number of animals in each quadrant was scored after 20 min, and the chemotaxis index was calculated as (the number of animals on ascaroside quadrants – the number of animals on control quadrants)/(the number of animals on ascaroside quadrants + the number of animals on control quadrants).

Optogenetics. L4 animals expressing Chr2 in RMG²⁷ were picked 24 h before the assay and divided into two groups. One group was transferred to plates that had 100 µl of 5 mM all-trans-Retinal (Sigma) in 100% ethanol added to the bacterial lawn. The other group was put on plates with 100 µl of ethanol as controls. Test and control plates were kept in the dark until animals were picked to assay plates 2 h before recording. Videos were recorded using a Grasshopper camera (Point Grey) mounted on an M165FC Stereo microscope (Leica) fitted with GFP excitation filters (ET 480/40 nm). Excitation light attenuated to 11.6 mW/cm² was from a Leica EL6000 mercury lamp. Animals were recorded for 4 min without the blue light stimulus, followed by 4 min of blue light stimulation and a further 4 min without blue light. O₂ (7%) was pumped into the microfluidic chamber throughout the assay. To record behaviour, we used trans-illumination, with light filtered through a 595-nm long-pass optical cast plastic filter (Edmund Optics).

Molecular biology. Expression plasmids were constructed using multisite Gateway (Life Technologies). Promoters used included *ilc-17.1* (6 kb), *ilcr-1* (6.5 kb), *ilcr-2* (2.4 kb), *npr-1*, *flp-5*, *flp-6*, *vha-6*, *ges-1*, *hsp-16.41*, *acr-2*, *glr-1*, *nmr-1*, *unc-17*, *unc-25*, *pik-1* (2.5 kb), *actl-1* (7 kb), and *nfki-1* (5.7 kb). For rescue experiments, cDNA for each gene was amplified using a Phusion RT-PCR kit (Thermo Scientific) and cloned into pDonor 221.

Primers for *ilc-17.1* cDNA amplification were GGGGACAAGTTTGTACAAA-AAAGCAGGCTTTTCAGAAAAATGCCAAAATCACCACACAGGAC and GGGGACCCTTTGTACAAGAAAGCTGGGTATTAATTTGGAATTTCTGCTTTGATTGTGTAGATAAAG; for *ilcr-1* cDNA amplification, GGGGACAAGTTTGTACAAAAGCAGGCTTTTCAGAAAAATGTTTCTTCATTCGCTGCTCTTC and GGGGACCCTTTGTACAAGAAAGCTGGGTATCAGTGTATACC AATGACTTTCATCATGGAAC; for *ilcr-2* cDNA amplification, GGGGACAAGTTTGTACAAAAGCAGGCTTTTCAGAAAAATGTTTCCGCTTTGCATACCA and GGGGACCCTTTGTACAAGAAAGCTGGGTATCATGACTTCTTCA CAACAATCGTCTTCG; for *pik-1* cDNA amplification, GGGGACAAGTTTGTACAAAAGCAGGCTTTTCAGAAAAATGGATGATTTCTTTGGAGTATCAGAAGTTG and GGGGACCCTTTGTACAAGAAAGCTGGGTATTA GACAACCTGGCGGAATTGAATTTTACA; for *actl-1* cDNA amplification,

GGGGACAAGTTTGTACAAAAGCAGGCTTTTCAGAAAAATGACTAA GATGAAAATGGACGTAACAATTGAG and GGGGACCCTTTGTAC AAGAAAGCTGGGTATTATTGTGTAATACTGTAGTTCATGGAATCCTCG; and for *nfki-1* cDNA amplification, GGGGACAAGTTTGTACAAAAGCAGGCTTTTCAGAAAAATGGCAACCGTTGCCCCCAAG and GGGGACCCTTTGTACAAGAAAGCTGGGTATCAAGCTCTCGACTTGTTCGGGACTG. To generate a functional *mcherry-ilc-17.1* transgene, mCherry coding sequences were inserted after the signal sequence between codons 31 and 32 of the *ilc-17.1* gene.

To express *C. elegans* proteins in HEK293T cells, cDNAs for each gene were amplified with primers that had a 25-base overlap with sequences in pcDNA vectors and assembled with the vector using the Gibson Assembly kit (New England Biolabs). The *ilc-17.1* cDNA without a signal sequence (that is, after codon 31) was cloned into a pcDNA5 vector that had the prolactin signal sequence, 3× Flag, and tobacco etch virus (TEV) cleavage site for amino (N)-terminal fusion. The *ilcr-1* cDNA was assembled in a pcDNA4 plasmid with EGFP sequences inserted between NarI and XbaI sites. The *ilcr-2* cDNA was assembled in a pcDNA4 vector that had sequences encoding TEV-3× HA right after the XbaI site and in a pcDNA4 plasmid with EGFP sequences inserted between NarI and XbaI sites. The *actl-1* cDNA was assembled to a pcDNA4 vector that had sequences encoding TEV-3× HA right after the XbaI site. The *pik-1* cDNA was assembled in a pcDNA4 vector with TEV-3× Flag for C-terminal tagging.

To tag *ilcr-2* with GFP while including long stretches of 5' and 3' sequences, we used fosmid recombineering⁴⁴. The GFP coding sequence was amplified using primers AATCCGACAATGAGGGTGAAGATCCGAAGACGATTGTTG TGAAGAAGTCAATGAGTAAAGGAGAAGAAGCTTTTCAC and GTATCACACCGTAACAAGCAATAAGCAAATAAAAATAACAAGTCTCTTCATTT GTATGTTTCATCCATGCCATG. The recombineerone site was confirmed by sequencing.

Transgenic animals were generated by injecting 50 ng/µl of the expression vector with 50 ng/µl of a coelomocyte-specific *punc-122::mcherry* marker. Mos-1-mediated single-copy gene insertion was performed as described²¹.

Protein sequence alignment. Alignments used T-coffee with default settings in Jalview. The blue shadow indicates the conservation score of residues.

Microscopy. Animals were immobilized using 50 mM sodium azide on 2% agarose pads in M9 buffer. Image acquisition and analysis were performed as described⁴⁵.

Heat-shock experiments. Strains were grown at 15 °C, to minimize leaky expression from the *hsp-16.41* promoter. To heat-shock animals, NGM plates were wrapped with parafilm and immersed in a 34 °C water-bath for 15 or 30 min. Animals were transferred to assay plates immediately after heat-shock. The same groups of animals were assayed every 2 h for 10 h for their responses to O₂ switches. mCherry expression was measured using an AZ100 microscope (Nikon) fitted with a 553/25 nm excitation filter and a 641/75 nm emission filter. Twenty-four animals were analysed for each time point and mCherry signals were captured from the whole animal using a 2× lens. Data were analysed using Image J.

Ca²⁺ imaging. L4 animals expressing the sensor were picked 24 h before imaging. Freely moving animals were imaged on plates containing NGM⁴¹ modified to minimize background fluorescence by omitting peptone and replacing agar with agarose (Fisher, BP164-100). Plates were dried on the bench overnight and, just before use, spotted with 3 µl of M9-washed and concentrated OP50 bacteria (grown in 10 ml 2×TY to an absorbance at 600 nm (*A*_{600nm}) = 1, spun and resuspended in 1 ml M9) to form a lawn of 5 mm diameter. Animals were picked to the plates, covered by the same microfluidic device used in our behavioural experiments, and allowed to roam freely while we imaged. The O₂ stimulus regime was identical to that in the behaviour analysis. Animals were imaged on an AZ100 microscope (Nikon) bearing a TwinCam adaptor (Cairn Research, UK) mounted with two ORCA-Flash4.0 V2 digital cameras (Hamamatsu, Japan) using an AZ Plan Fluor 2× lens with 2× zoom and an exposure time of 100 ms. The excitation light was passed through a 438/24 nm filter and an FF458-DiO2 dichroic (Semrock) and attenuated to 4.39 mW/cm², a light intensity that did not change worm behaviour. The TwinCam adaptor cube was mounted with cyan fluorescent protein (483/32 nm) and yellow fluorescent protein (542/27 nm) emission filters and a DC/T510LPXRT-Uf2 dichroic. Animals were imaged twice, after 10 min and 2 h on the assay plates. Imaging data were analysed using Neuron Analyzer, a custom-written Matlab program, to analyse the resulting image stacks (code available at <https://github.com/neuronanalyser/neuronanalyser>).

Ca²⁺ imaging of glued animals used the same hardware and settings, except that a 500-ms exposure time was used. Five or six animals were glued simultaneously onto a 2% agarose pad in M9 on a glass slide, and a small amount of food placed close to their nose. The animals were quickly covered by the microfluidic chamber and 7% O₂ pumped into the chamber for 1 min before we started imaging.

To image Ca²⁺ responses to pheromone and benzaldehyde, we used olfactory chips (Microkosmos, <https://www.ukosmos.com/>) as previously described⁴⁶.

Ascaroside (100 nM) and 10^{-4} diluted benzaldehyde (diluted in M13 buffer) were used to assess RMG and AIB responses respectively.

Immunofluorescence for mammalian cells. HEK293T cells used in this study were obtained from American Type Culture Collection (ATCC CRL-3216) and were tested for mycoplasma infection. Cells were cultivated at 37°C, except when ILKR-2 was being expressed. Proper folding and surface expression of ILKR-2 required analysis at 32°C. Cells grown on coverslips were washed with PBS and fixed in 3.7% formaldehyde in PBS for 15 min. Fixed cells were permeabilized with 0.1% Triton X-100 in PBS for 5 min, blocked with 10% fetal bovine serum in PBS for 30 min, and incubated with primary antibodies for 1 h. After washing, cells were incubated with AlexaFluor 546-conjugated goat anti-mouse IgG (Invitrogen) for 60 min. Images were acquired on an LSM 780 (Zeiss) using a 63× numerical aperture 1.42 oil-immersion objective lens.

Immunoprecipitation and immunoblotting. Cell lysates were prepared in lysis buffer (50 mM Tris-HCl pH 7.5, 150 mM NaCl, 1% CHAPS, 1 mM phenylmethanesulfonyl fluoride (PMSF) and protease inhibitor cocktail (complete EDTA-free protease inhibitor, Roche)), clarified by centrifugation at 15,000 r.p.m., and subjected to immunoprecipitation using anti-HA agarose (Sigma A2095), anti-Flag M2 affinity gel (Sigma A2220), or GFP-Trap A (Chromotek). Precipitated immunocomplexes were washed five times in a washing buffer (50 mM Tris-HCl pH 7.5, 150 mM NaCl, 1 mM EDTA, and 1% CHAPS) and boiled in sample buffer. Samples were separated by SDS-PAGE and transferred to nitrocellulose membranes (Biorad). Immunoblot analysis was performed with anti-Flag M2 (F3165), anti-GFP⁴⁷, and anti-HA (clone 16B12), and visualized with Super Signal West Pico Chemiluminescent substrate (Pierce). Immunoblot images of chemiluminescent signals were acquired using the Bio-Rad Geldoc system. Acquired images were saved at the highest resolution. The software automatically highlights saturated pixels and marks them with small black squares, which is why such regions of the image appear pixelated. To visualize faint bands in some blots, parts of the intense bands become over-exposed and generate the observed pixellation. Our conclusions are not affected by this.

Purification of Flag-ILC-17.1. Conditioned medium from Flp-In T-Rex HEK293 cells stably expressing Flag-ILC-17.1 was collected and concentrated in Amicon Ultra filtration units (Millipore). Flag-ILC-17.1 was immunoprecipitated using

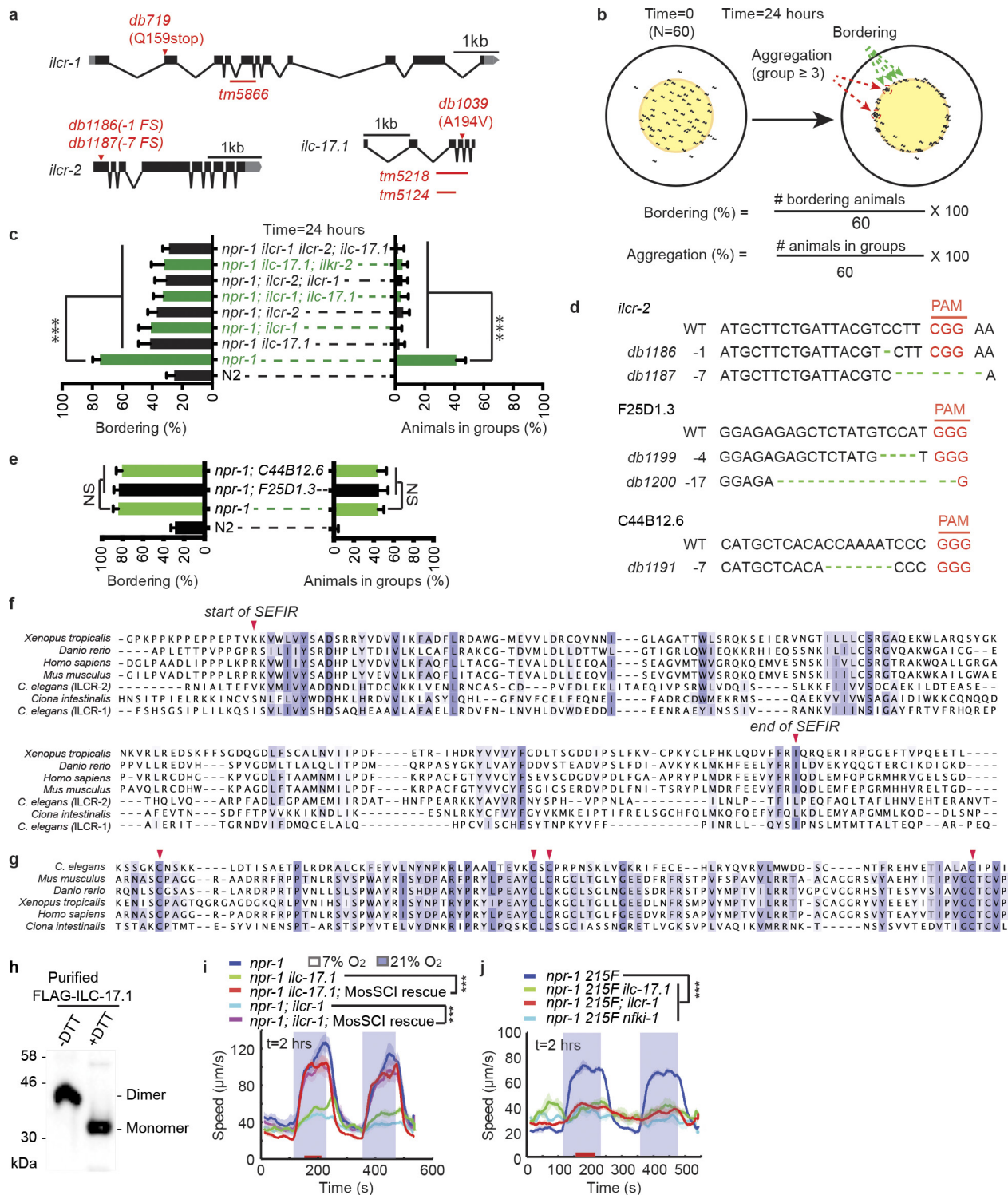
anti-Flag M2 agarose (Sigma), washed with wash buffer (110 mM KAc, 20 mM HEPES pH 7.4, and 2 mM MgCl₂) and eluted using 0.25 mg/ml 3× Flag-peptide in PBS.

Flow cytometry analysis. Transfected HEK293T cells were detached with EDTA and kept on ice during the whole staining procedure. Cells were incubated in 10% FBS/PBS containing 0.05 ng/μl purified Flag-ILC-17.1 for 30 min at 4°C. The Flag tag was detected with the anti-Flag M2 antibody and AlexaFluor 546-conjugated goat anti-mouse IgG. Stained cells were washed in PBS, re-suspended in 10% FBS/PBS with 1 μg/ml DAPI, and analysed using a flow cytometer (LSRII, BD Biosciences).

Code availability. Zentracker, the custom-written Matlab software used to analyse worm movies, is available at <https://github.com/wormtracker/zentracker>. Neuron Analyzer, the custom-written Matlab program used to analyse neural image stacks, is available at <https://github.com/neuronanalyser/neuronanalyser>.

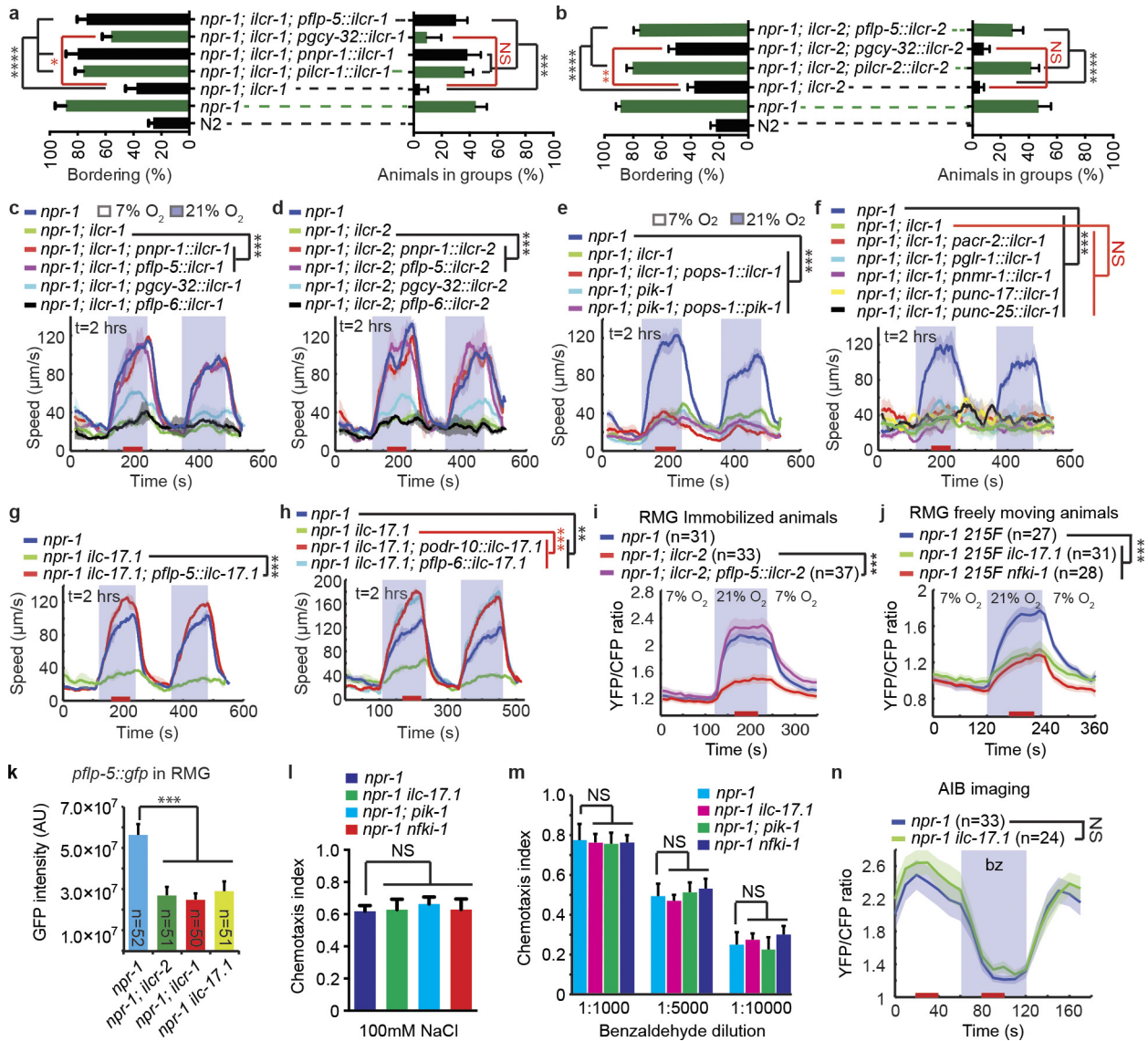
Data availability. The data that support the findings of this study are available from the corresponding author.

41. Sulston, J. & Hodgkin, J. in *The Nematode Caenorhabditis elegans* (ed. Wood, W. B.) 587–606 (Cold Spring Harbor Laboratory Press, 1988).
42. Chen, C., Fenk, L. A. & de Bono, M. Efficient genome editing in *Caenorhabditis elegans* by CRISPR-targeted homologous recombination. *Nucleic Acids Res.* **41**, e193 (2013).
43. de Bono, M. & Bargmann, C. I. Natural variation in a neuropeptide Y receptor homolog modifies social behavior and food response in *C. elegans*. *Cell* **94**, 679–689 (1998).
44. Tursun, B., Cochella, L., Carrera, I. & Hobert, O. A toolkit and robust pipeline for the generation of fosmid-based reporter genes in *C. elegans*. *PLoS ONE* **4**, e4625 (2009).
45. Chen, C., Itakura, E., Weber, K. P., Hegde, R. S. & de Bono, M. An ER complex of ODR-4 and ODR-8/Ufm1 specific protease 2 promotes GPCR maturation by a Ufm1-independent mechanism. *PLoS Genet.* **10**, e1004082 (2014).
46. Chronis, N., Zimmer, M. & Bargmann, C. I. Microfluidics for *in vivo* imaging of neuronal and behavioral activity in *Caenorhabditis elegans*. *Nature Methods* **4**, 727–731 (2007).
47. Stefanovic, S. & Hegde, R. S. Identification of a targeting factor for posttranslational membrane protein insertion into the ER. *Cell* **128**, 1147–1159 (2007).



Extended Data Figure 1 | Interleukin-17-related proteins and receptors in *C. elegans*. **a**, Schematic of the exon/intron structures of the *Y64G10A.6* (*ilcr-1*), *F56D1.2* (*ilcr-2*), and *T22H6.1* (*ilcr-17.1*) genes, with the location of mutations used in assays indicated. The terms -1 FS and -7 FS denote frameshift mutations with 1 and 7 base pair deletions. Other alleles are shown in Extended Data Table 1. **b**, Schematic showing the bordering and aggregation assay. The number of animals on the edge of the food lawn, or in groups, was counted 24 h after animals were transferred to the assay plates. **c**, Bordering and aggregation phenotypes of single-, double-, and triple-null mutants of *ilcr-17.1*, *ilcr-1*, and *ilcr-2*; *n* = 4 assays; ****P* < 0.001, ANOVA with Tukey correction. **d**, CRISPR induced mutations in the *F56D1.2* (*ilcr-2*) gene, and the *F25D1.3* and *C44B12.6* genes, which show homology to mammalian IL-17. **e**, Bordering and

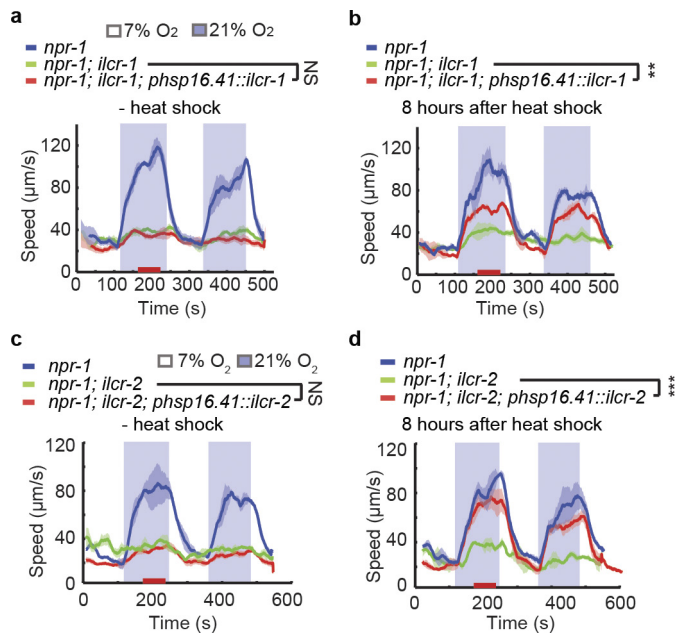
aggregation assays for the *F25D1.3* and *C44B12.6* mutants; *n* = 4 assays. NS, not significant (ANOVA with Tukey correction). **f**, Alignment of the SEFIR domains of IL-17 receptors, including *C. elegans* ILCR-1 and ILCR-2. **g**, Alignment of IL-17D proteins with IL-17.1. Arrowheads indicate conserved cysteine residues. **h**, ILC-17.1 forms disulfide-linked dimers. SDS-PAGE of affinity-purified Flag-ILC-17.1 boiled in sample buffer with or without 100 mM DTT. **i**, The O₂ response defects of *ilcr-17.1* and *ilcr-1* mutants are rescued by Mos1-mediated single copy insertion (MosSCI) of *ilcr-17.1* and *ilcr-1* transgenes; *n* = 4 assays, 120 animals. ****P* < 0.001, Mann-Whitney *U*-test. **j**, The O₂ response defects of *ilcr-17.1*, *ilcr-1*, and *nfki-1* double mutants with the natural *npr-1* 215F allele; *n* = 4 assays, 120 animals. ****P* < 0.001, Mann-Whitney *U*-test.



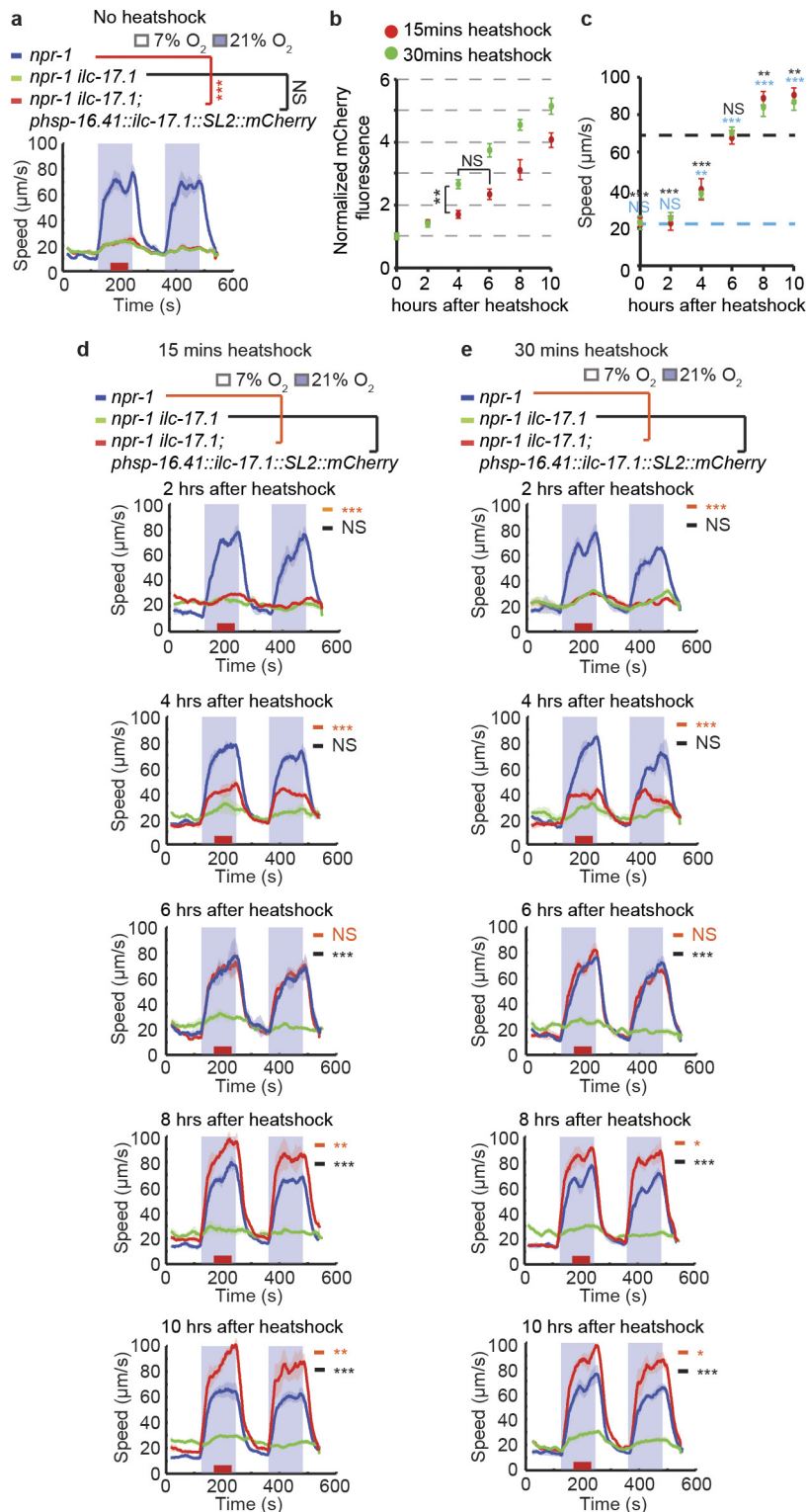
Extended Data Figure 2 | ILC-17.1 signalling in RMG promotes aggregation and escape from 21% O₂.

a, b, The bordering and aggregation defects of *ilcr-1* and *ilcr-2* mutants can be rescued by selectively expressing their cDNAs in RMG interneurons (*pnpr-1* and *pflp-5*). Bordering but not aggregation is partly rescued by expression in the O₂-sensing neurons URX, AQR, and PQR (*pgcy-32*); *n* = 4 assays. **P* < 0.05, ***P* < 0.01, *****P* < 0.0001, ANOVA with Tukey correction. **c, d**, O₂ responses of *ilcr-1* (**c**) and *ilcr-2* (**d**) mutants expressing the corresponding cDNA selectively in RMG (*pnpr-1* and *pflp-5*), the O₂ sensing neurons URX, AQR, and PQR (*pgcy-32*), or the ASE gustatory neurons (*pflp-6*); *n* = 4 assays, 120 animals. ****P* < 0.001, Mann-Whitney *U*-test. **e**, Expressing *ilcr-1* or *pik-1* cDNA in ASG neurons, using the *ops-1* promoter, fails to rescue the O₂ response defects of the corresponding mutants; *n* = 4 assays, 120 animals. ****P* < 0.001, Mann-Whitney *U*-test. **f**, Expressing *ilcr-1* cDNA in cholinergic neurons (*punc-17* or *pacr-2*), GABAergic neurons (*punc-25*), or interneurons controlling forward and reverse movement (*pglr-1*, *pnmr-1*) fails to restore sustained locomotory arousal to *ilcr-1* mutants kept at 21% O₂; *n* = 4 assays, 120 animals. ****P* < 0.001, Mann-Whitney *U*-test. **g**, Expressing *ilcr-17.1* cDNA in RMG using the *pflp-5* promoter rescues defective

responses to 21% O₂ in *ilcr-17.1* mutants. Speed assays were performed 2 h after animals were transferred to the assay plates; *n* = 4 assays, 120 animals. ****P* < 0.001, Mann-Whitney *U*-test. **h**, Expressing *ilcr-17.1* cDNA from the *odr-10* promoter (AWA) or the *pflp-6* promoter (ASE) not only rescues the *ilcr-17.1* defect but confers abnormally heightened escape from 21% O₂; *n* = 4 assays, 120 animals. ***P* < 0.01, ****P* < 0.001, Mann-Whitney *U*-test. **i**, Expressing *ilcr-2* cDNA using the *pflp-5* promoter rescues the RMG O₂-evoked Ca²⁺ responses defects of *ilcr-2* mutants. ****P* < 0.001, Mann-Whitney *U*-test. The *npr-1* control is the same as in Fig. 4e. **j**, The *ilcr-17.1*; *npr-1* 215F and *nfki-1*; *npr-1* 215F mutants show defective O₂-evoked Ca²⁺ response in RMG; *npr-1* 215F is the allele found in natural isolates of *C. elegans*. ****P* < 0.001, Mann-Whitney *U*-test. **k**, Expression of *pflp-5::GFP* in RMG interneurons, a reporter of RMG neurosecretory activity, is reduced in *ilcr-17.1*, *ilcr-1*, and *ilcr-2* mutants. ****P* < 0.001, ANOVA with Tukey correction. **l, m**, The *ilcr-17.1*, *pik-1*, and *nfki-1* mutants display normal chemotaxis to NaCl (**l**) and benzaldehyde (**m**); *n* = 6 assays. NS, not significant, ANOVA with Tukey correction. **n**, Ca²⁺ responses evoked in AIB interneurons by benzaldehyde (1:10,000 dilution) are normal in *ilcr-17.1* mutants; bz, benzaldehyde; Mann-Whitney *U*-test.

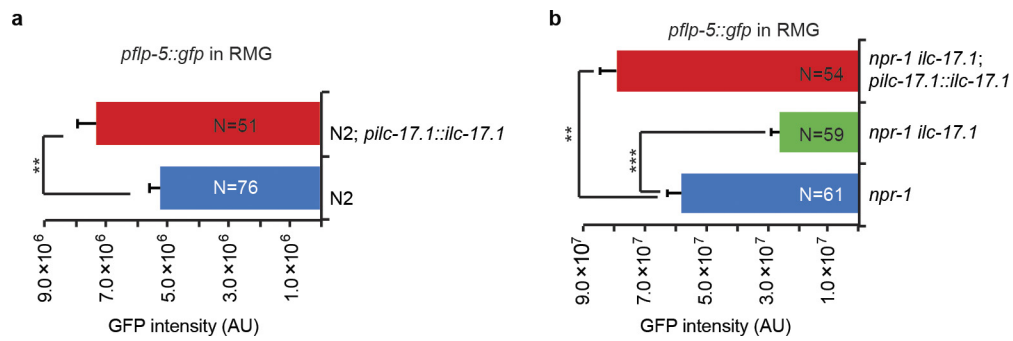


Extended Data Figure 3 | Heat-shock-induced expression of ILCR-1 and ILCR-2 in adults rescues behavioural defects of corresponding mutants. **a–d**, Transgenic adults expressing *ilcr-1* cDNA (**a, b**) or *ilcr-2* cDNA (**c, d**) from the *hsp-16.41* promoter were assayed either without heat-shock (**a, c**) or after 30 min of heat-shock (**b, d**). The assays in **b** and **d** were performed 8 h after the heat-shock; $n = 4$ assays, 120 animals. $**P < 0.01$, $***P < 0.001$, NS, not significant, Mann–Whitney U -test.

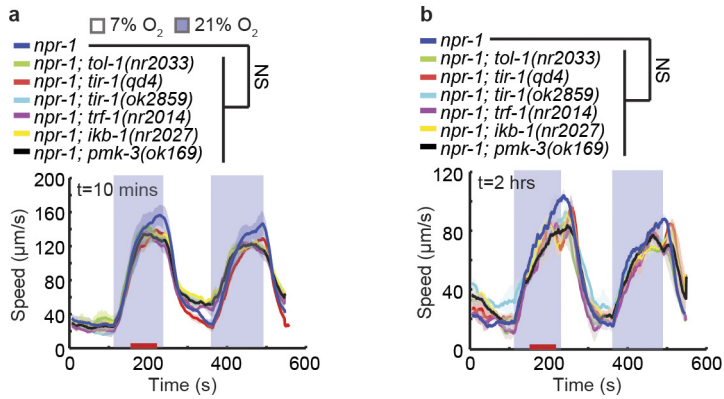


Extended Data Figure 4 | Timeline of heat-shock-induced rescue of *ilc-17.1* after 15- and 30-min heat shocks. **a**, The *ilc-17.1* mutants expressing *ilc-17.1* cDNA from the *hsp-16.41* promoter assayed without heat shock. Assays were performed 2 h after animals were picked to assay plates; $n = 4$ assays, 120 animals. $***P < 0.001$, Mann–Whitney U -test. **b**, **c**, Timelines showing mCherry expression (**b**) and speed at 21% O₂ (**c**) of *ilc-17.1* mutants bearing a *phsp-16.41::ilc-17.1::mChery* bicistronic transgene and heat shocked for 15 or 30 min. For each mCherry measurement, $n = 24$; speed in **c** is the average of a 1-min time window, 40 s after switching to 21% O₂ and 20 s before switching back to 7% O₂, indicated with a red bar in **d** and **e**. The dashed lines in **c** indicate the average speed of *npr-1* (black)

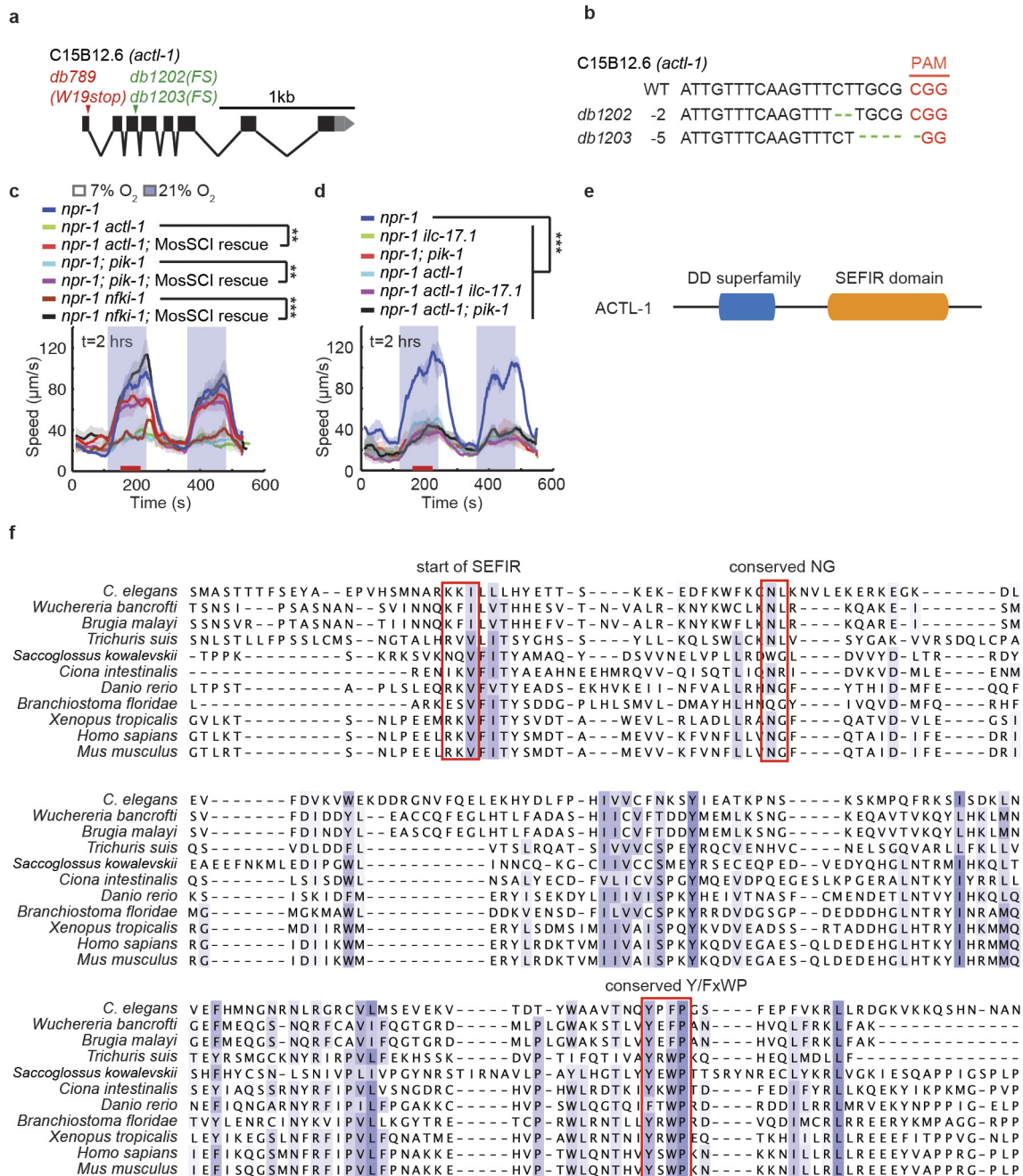
and *ilc-17.1 npr-1* (blue) animals for comparison. $**P < 0.01$, $***P < 0.001$, Mann–Whitney U -test; P values in black are for comparisons with *npr-1* control; P values in blue are for comparisons with *ilc-17.1 npr-1* controls. **d**, **e**, Transgenic animals expressing *ilc-17.1* cDNA from the *hsp-16.41* promoter were exposed to 34 °C for 15 min (**d**) or 30 min (**e**), then assayed every 2 h. Statistical comparisons between *npr-1* and transgenic animals with heat-shock constructs are indicated in orange. Comparisons between *npr-1 ilc-17.1* and transgenic animals with heat-shock constructs are indicated in black; $n = 4$ assays, 120 animals. $***P < 0.001$, $**P < 0.01$, $*P < 0.05$, Mann–Whitney U -test.



Extended Data Figure 5 | Overexpressing ILC-17.1 stimulates *flp-5* neuropeptide expression in RMG. a, b, Overexpressing *ilc-17.1* stimulates expression from the *pflp-5::GFP* reporter in RMG both in N2 (a) and *npr-1* (b) animals. Conversely, disrupting *ilc-17.1* reduces *pflp-5::gfp* expression. ** $P < 0.01$, *** $P < 0.001$, Mann-Whitney U -test.

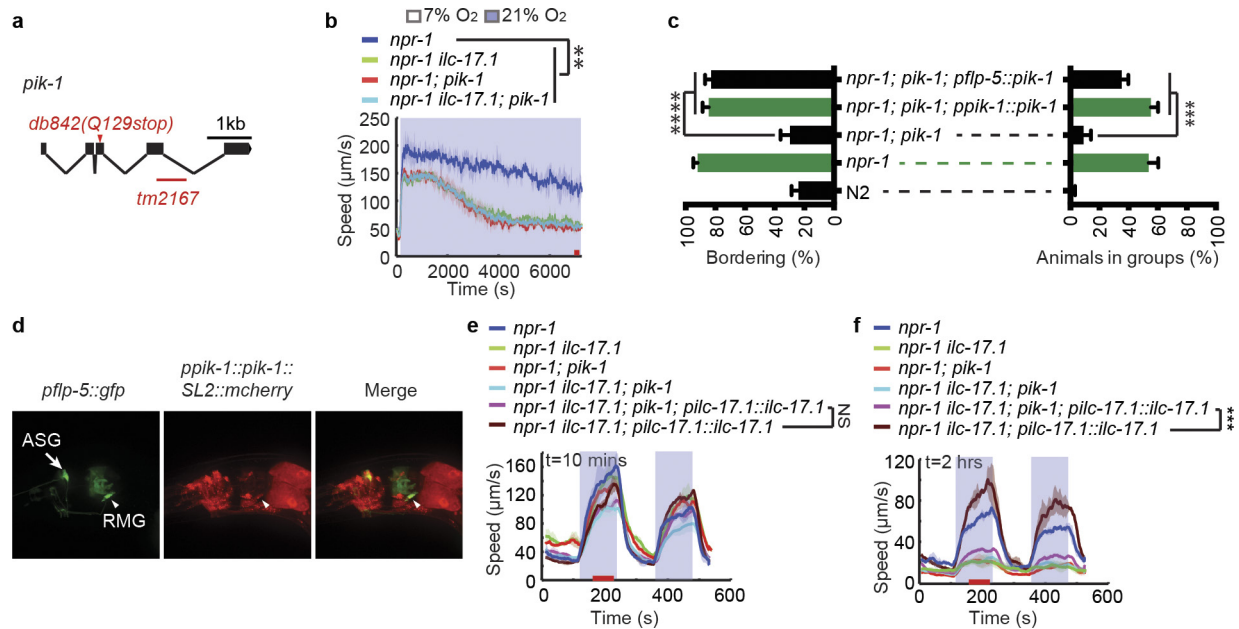


Extended Data Figure 6 | Phenotypes of *C. elegans* homologues of mammalian genes involved in inflammatory responses. a, b, Speed was assayed 10 min (a) and 2 h (b) after animals were transferred to the assay plates; $n = 4$ assays, 120 animals. NS, not significant, Mann-Whitney U -test.



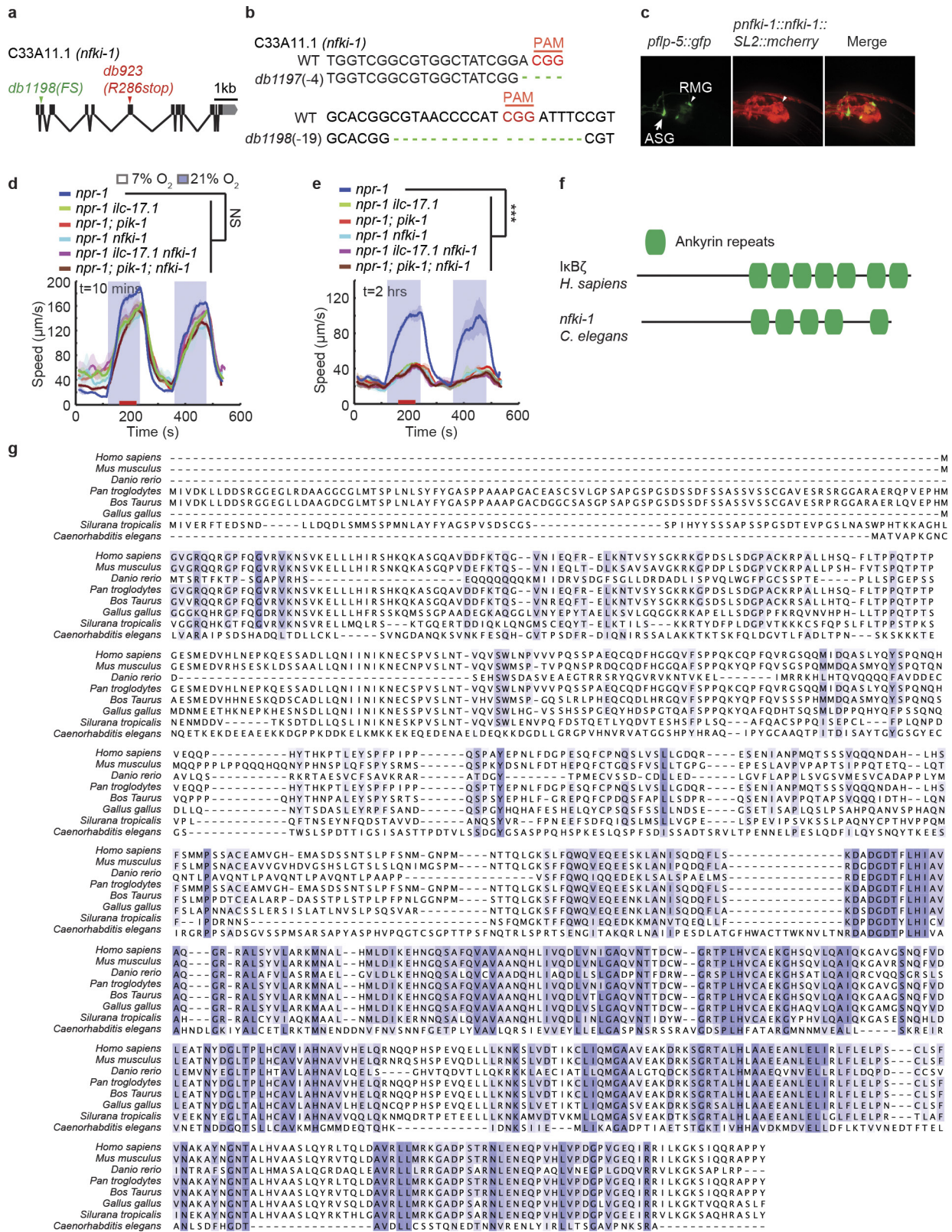
Extended Data Figure 7 | The *C. elegans* Act1-like gene. **a, b**, The *actl-1* alleles. Allele *db789* was isolated in strain AX3544 after mutagenesis using ethylmethanesulfonate (EMS) (**a**); *db1202* and *db1203* are frameshift mutations generated by CRISPR (**b**). **c**, Mos1-mediated single-copy insertion (MosSCI) of the *actl-1*, *pik-1*, and *nfki-1* genes rescues the O₂ response defects of the corresponding mutants; *n* = 4 assays, 120 animals. ****P* < 0.001, ***P* < 0.01, Mann-Whitney *U*-test. **d**, A null mutation

in *actl-1* confers *ilc-17.1*-like responses to 21% O₂, and does not show additive phenotypes with *ilc-17.1* or *pik-1* null mutations; *n* = 4 assays, 120 animals. ****P* < 0.001, Mann-Whitney *U*-test. **e**, Domain architecture of ACTL-1, showing the locations of the Death and SEFIR domains. **f**, Alignment of the SEFIR domains of ACT1 and ACT1-like proteins. *C. elegans* ACTL-1 is shown at the top.



Extended Data Figure 8 | Disrupting *pik-1*/IRAK causes *ilc-17.1*-like phenotypes. **a**, Schematic of the exon/intron structure of *pik-1*, highlighting the *db842* and *tm2167* mutations used in this study. The allele *db842* was found in strain AX3604; *tm2167* was obtained from the Japanese knockout consortium. **b**, The *pik-1* mutants exhibit an *ilc-17.1*-like defect and fail to sustain rapid movement at 21% O_2 . The *pik-1* and *ilc-17.1* phenotypes are non-additive, suggesting the proteins encoded by these genes act in the same pathway; $n = 4$ assays, 120 animals. $**P < 0.01$, Mann–Whitney U -test. **c**, The bordering and aggregation defects of *pik-1*

mutants can be rescued by expressing *pik-1* cDNA from the *pik-1* or *pflp-5* promoters (RMG); $n = 4$ assays. $***P < 0.001$, $****P < 0.0001$, Mann–Whitney U -test. **d**, A functional *ppik-1::pik-1::SL2::mCherry* polycistronic transgene is expressed broadly in the nervous system. RMG expression was confirmed using a *pflp-5::gfp* fiduciary marker. **e**, **f**, Sustained rapid movement of *ilc-17.1* overexpressing animals at 21% O_2 is blocked by mutations in the *pik-1* gene. Speed assays were performed 10 min (**e**) and 2 h (**f**) after picking animals to the assay plates; $n = 4$ assays, 120 animals. $***P < 0.001$, Mann–Whitney U -test.



Extended Data Figure 9 | Mutations in the *nfki-1* gene cause *ilc-17.1*-like phenotypes. a, b, The *nfki-1* alleles. Allele *db923* in strain *AX3677* was obtained in an EMS screen (a); the *db1198* frameshift mutation was generated using CRISPR (b). c, A functional *pnfki-1::nfki-1::SL2::mCherry* polycistronic transgene is expressed broadly in the nervous system. RMG expression was confirmed using a *pflp-5::gfp* fiducial marker.

d, e, Phenotypes of *nfki-1*, *pik-1*, and *ilc-17.1* molecular null alleles are not additive; *n* = 4 animals, 120 animals. **P* < 0.001, Mann-Whitney *U*-test. **f**, Schematic of the human $\text{IkB}\zeta$ b isoform and NFKI-1, highlighting ankyrin repeats (ANK). **g**, Alignment of amino-acid sequences for $\text{IkB}\zeta$ orthologues from different species. NFKI-1 is shown at the bottom. Conserved residues are highlighted.**

Extended Data Table 1 | Mutations in IL-17 signalling components identified by forward genetics

Gene	Strain	Position	Reference	Alteration	Effect	aa change
<i>ilcr-1</i>	AX3344	14278292	C	T	STOP_GAINED	Q159*
	AX3378	14283135	C	T	STOP_GAINED	R548*
	AX3582	14280894	C	T	NON_SYNONYMOUS_CODING	S487F
	AX3667	14279516	TCC	TC	FRAME_SHIFT	-277
	AX3696	14279564	C	T	NON_SYNONYMOUS_CODING	P292L
	AX3836	14279479	C	T	STOP_GAINED	Q264*
<i>ilc-17.1</i>	AX3589	12768673	C	T	SPLICE_SITE_DONOR	/
	AX3617	12767526	C	T	NON_SYNONYMOUS_CODING	G207R
	AX3801	12767612	G	A	NON_SYNONYMOUS_CODING	A194V
	AX3699	12767680	C	T	SPLICE_SITE_ACCEPTOR	/
<i>actl-1</i>	AX3295	6497190	C	T	NON_SYNONYMOUS_CODING	S324N
	AX3544	6499781	C	T	STOP_GAINED	W19*
<i>pik-1</i>	AX3273	13417889	G	A	STOP_GAINED	W30*, W70*
	AX3596	13418117	C	T	STOP_GAINED	Q129*, Q89*
	AX3604	13419353	GAAATGATACA TCACAGAA	GA	FRAME_SHIFT	-220, -180
<i>nfski-1</i>	AX3301	15357365	C	T	STOP_GAINED	Q179*
	AX3792	15357721	A	G	NON_SYNONYMOUS_CODING	D247G
	AX3677	15359285	C	T	STOP_GAINED	R286*